CORA Cork Open Research Archive
Cartlann Taighde Oscailte Chorcaí

Title	Non-classical behaviour of higher valence dopants in chromium (III) oxide by a Cr vacancy compensation mechanism
Authors	Carey, John J.;Nolan, Michael
Publication date	2017-09-05
Original Citation	Carey, J. J. and Nolan, M. (2017) 'Non-classical behaviour of higher valence dopants in chromium (III) oxide by a Cr vacancy compensation mechanism', Journal of Physics: Condensed Matter, 29(41), 415501 (14pp). doi:10.1088/1361-648X/aa8250
Type of publication	Article (peer-reviewed)
Link to publisher's version	10.1088/1361-648X/aa8250
Rights	© 2017 IOP Publishing Ltd. This is an author-created, un-copyedited version of an article accepted for publication/ published in Journal of Physics: Condensed Matter. IOP Publishing Ltd is not responsible for any errors or omissions in this version of the manuscript or any version derived from it. The Version of Record is available online at http://dx.doi.org/10.1088/1361-648X/aa8250
Download date	2026-11-06 18:55:48
Item downloaded from	https://hdl.handle.net/10468/4675

UCC
University College Cork, Ireland
Coláiste na hOllscoile Corcaigh

IOPscience iopscience.iop.org

Home Search Collections Journals About Contact us My IOPscience

Non-classical behaviour of higher valence dopants in chromium (III) oxide by a Cr vacancy compensation mechanism

This content has been downloaded from IOPscience. Please scroll down to see the full text.

Download details:

IP Address: 143.239.102.147
This content was downloaded on 02/08/2017 at 12:35

Manuscript version: Accepted Manuscript
Carey et al

To cite this article before publication: Carey et al, 2017, J. Phys.: Condens. Matter, at press:
https://doi.org/10.1088/1361-648X/aa8250

This Accepted Manuscript is: © 2017 IOP Publishing Ltd

During the embargo period (the 12 month period from the publication of the Version of Record of this article), the Accepted Manuscript is fully protected by copyright and cannot be reused or reposted elsewhere.

As the Version of Record of this article is going to be / has been published on a subscription basis, this Accepted Manuscript is available for reuse under a CC BY-NC-ND 3.0 licence after the 12 month embargo period.

After the embargo period, everyone is permitted to copy and redistribute this article for non-commercial purposes only, provided that they adhere to all the terms of the licence
https://creativecommons.org/licences/by-nc-nd/3.0

Although reasonable endeavours have been taken to obtain all necessary permissions from third parties to include their copyrighted content within this article, their full citation and copyright line may not be present in this Accepted Manuscript version. Before using any content from this article, please refer to the Version of Record on IOPscience once published for full citation and copyright details, as permission will likely be required. All third party content is fully copyright protected, unless specifically stated otherwise in the figure caption in the Version of Record.

When available, you can view the Version of Record for this article at:
http://iopscience.iop.org/article/10.1088/1361-648X/aa8250

Non-classical behaviour of higher valence dopants in chromium (III) oxide by a Cr vacancy compensation mechanism

John J Carey, and Michael Nolan*

*Corresponding author: Michael.nolan@tyndall.ie

Tyndall National Institute, University College Cork, Lee Maltings Complex, Cork, Ireland

Abstract

Modification of metal oxides with dopants that have a stable oxidation in their parent oxides which is higher than the host system is expected to introduce extra electrons into the material to improve carrier mobility. This is essential for applications in catalysis, SOFCs and solar energy materials. Density functional theory calculations are used to investigate the change in electronic and geometric structure of chromium (III) oxide by higher valence dopants, namely; Ce, Ti, V and Zr. For single metal doping, we find that the dopants with variable oxidation states, Ce, Ti and V, adopt a valence state of +3, while Zr dopant has a +4 oxidation state and reduces a neighbouring Cr cation. Chromium vacancy formation is greatly enhanced for all dopants, and favoured over oxygen vacancy formation. The Cr vacancies generate holes which oxidise Ce, Ti and V from +3 to +4, while also oxidising lattice oxygen sites. For Zr doping, the generated holes oxidise the reduced Cr^{2+} cation back to Cr^{3+} and also two lattice oxygen atoms. Three metal atoms in the bulk lattice facilitate spontaneous Cr vacancy occurs from charge compensation. A non-classical compensation mechanism is observed for Ce, Ti and V; all three metals are oxidised from +3 to +4 which explains experimental observations that these metals have a +4 oxidation state in Cr_2O_3. Charge

Accepted Manuscript

compensation of the three Zr metals proceeds by a classical higher valence doping mechanism; the three dopants reduce three Cr cations, which are subsequently charge compensated by a Cr vacancy oxidising three Cr^{2+} to Cr^{3+}. The compensated structures are the correct ground state electronic structure for these doped systems, and used as a platform to investigate cation/anion vacancy formation. Unlike the single metal doped bulks, preference is now given for oxygen vacancy formation over Cr vacancy formation, indicating that the dopants increase the reducibility of Cr_2O_3 with Ce doping showing the strongest enhancement. The importance of the correct ground state in determining the formation of defects is emphasised.

1. Introduction

Chromium oxide is a reducible oxide with many different oxidation states from Cr^{2+} to Cr^{6+} that can crystallise in different phases of CrO, Cr_2O_3, Cr_2O_5 and CrO_3 with the corundum structure of chromium oxide (α-Cr_2O_3) that is shared with Al_2O_3, Ti_2O_3, α-Fe_2O_3 and V_2O_3.[1, 2] being the most thermodynamically stable phase at low temperatures and pressures.[3] Chromium (III) oxide crystallises in a hexagonal crystal structure with experimental lattice vectors of a=b=4.96Å and c=13.599Å, cell angles of $\alpha=\beta=90^{\circ}$ and $\gamma=120^{\circ}$ determined by x-ray diffraction,[4] and belongs to the $R\bar{3}c$ space group. The Cr^{3+} cations are coordinated to six oxygen anions in an octahedral geometry, while the oxygen anions have a tetrahedral geometry bonding to four Cr^{3+} cations. Cr_2O_3 is anti-ferromagnetic with a magnetic ground state structure of alternating '-+-+' Cr^{3+} layers throughout the material, similar to magnetic phases of Hematite,[5, 6] and is a dielectric with a wide fundamental band gap (> 3eV) that is half way between a Mott-Insulator and charge transfer semi-conductor,[7, 8] since the valence band maximum (VBM) and conduction band minimum (CBM) are a mixture of Cr 3d and O

Accepted Manuscript

2p state, characterised by electron-energy loss spectroscopy,[9] and x-ray photoemission spectroscopy.[10, 11] Cr_2O_3 has been a very useful material for a wide range of applications and extensively studied in oxygenation catalysis,[12-16] hydrogen generation,[17-19] high temperature methanol synthesis,[20-22] as an anode material for Li-ion battery applications,[23, 24] in gas sensors,[25-27] solid oxide fuel cells,[28] protective coatings[29, 30] and adhesion promoters.[31] The fundamental properties of Cr_2O_3 for these applications can be altered and potentially improved by substitutional doping of the lattice Cr sites with an aliovalent dopant species.

Substitutional doping of the host cation site can alter the electronic structure and transport properties of the material, and promote different charge carrier mechanisms, such as lattice oxygen vacancy formation and mobility. This approach has been extensively used to improve the material properties of interest, for example photocatalytic activity of TiO_2[32-39] and enhancing the oxygen vacancy formation and storage capacity (OSC) of CeO_2.[40-50] A dopant species that has a stable valance state in its parent oxide which is lower than its host oxide is termed a lower valence dopant, while a metal species that has a higher valence in its parent oxide is termed a higher valence dopant.

Doping has been used for Mg doping of Cr_2O_3 to improve the mobility of holes to greatly enhance the p-type conductivity in the material for optoelectronic devices,[51-53] and has been extensively studied by both theory and experiment.[54-59] Mg doping can enhance the conductivity of Cr_2O_3 and co-doping with Mg/N has also shown promising p-type behavior.[55] However the growth conditions, namely Cr-rich/O-poor or Cr-poor/O-rich, of Cr_2O_3 can play a key role in the appearance of p-type conductivity; Mg-Cr_2O_3 is p-type under Cr-rich/O-poor conditions as the Mg dopant is not charge compensated.[57] Charge compensation in lower valence doping of Cr_2O_3 occurs by spontaneous generation of oxygen vacancies that release electrons into the host by a reduction process, killing the holes. This is detrimental to p-type conductivity. However, consideration of charge compensating species is vital to correctly

Accepted Manuscript

describe the ground state electronic structure.[24, 40, 41, 60-62] If the system is not charge compensated the material is not charge neutral which can lead to issues in calculating properties, such as over-binding of electron rich adsorbates.

The introduction of higher valence dopants (HVD) in bulk metal oxides is expected to provide additional electrons into the material for improved electron carrier concentrations and mobility; an example of this would be a metal cation with a 4+ oxidation state that substitutionally replaces a Cr^{3+} cation on its lattice site. The classical, and generally accepted mechanism for this process is the creation of an effective positively charged site on the doped cation site, and the electron rich dopant can reduce neighbouring Cr^{3+} cations to Cr^{2+} (Cr'_{Cr}):

$$2Cr_{Cr}^{x} + \frac{1}{2}O_2 + Cr_{Cr}^{x} + MO_2 \rightarrow M_{Cr}^{\cdot} + Cr'_{Cr} + Cr_2O_3 \quad \text{(Reduction process)} \quad (3)$$

Where M is a HVD that has an oxidation state of +4, and $M_{Cr}^{\cdot}$ is the metal substituting a Cr^{3+} lattice site with an effective positive charge. The excess valence electron(s) from the HVD can then remain on the metal dopant lattice site or can reduce neighboring Cr cations from Cr^{3+} to Cr^{2+} by an electron hopping process (n-type conductivity), similar to the hole hopping mechanism (p-type conductivity) for LVDs in metal oxides.

As the system now has a positively charged dopant site ($M_{Cr}^{\cdot}$), a compensation process will charge balance the system by either formation of negatively charged defects such as Cr vacancies (V_{cr}''') or oxygen interstitials (O_i'') in a similar manner to charge balancing hole formation in LVDs by oxygen vacancy formation ($V_o^{\cdot\cdot}$).[40, 41, 62] The process of charge balancing for HVDs to so that overall charge neutral system is obtained takes place as follows:

$$3Cr_{Cr}^{x} + Cr_{Cr}^{x} + 3MO_2 \rightarrow 3M_{Cr}^{\cdot} + V_{Cr}''' + 2Cr_2O_3 \quad \text{(Chromium Vacancy Formation)} \quad (4)$$

$$2Cr_{Cr}^{x} + \emptyset + 2MO_2 \rightarrow 2M_{Cr}^{\cdot} + O_i'' + Cr_2O_3 \quad \text{(Oxygen Interstitial Formation)} \quad (5)$$

Accepted Manuscript

Where ∅ is an empty site in the bulk chromia lattice that can be occupied by an oxygen interstitial (O_i''). The Chromium vacancies compensate by creating hole states on local lattice oxygen species which are then filled by the extra electrons introduced into the system from the dopant species, while oxygen interstitials introduce holes into the system that can also be filled from the excess electrons. These charge compensating processes create charge neutral defect pairings, $[3M_{Cr}^{\cdot} + V_{Cr}'''']$ or $[2M_{Cr}^{\cdot} + O_i'']$, in a similar manner to Frenkel $[O_i'' + V_o^{\cdot\cdot}]$ and Schottky $[2V_{Cr}'''' + 3V_O^{\cdot\cdot}]$ neutral defects that can occur in undoped chromia, where DFT calculations show that Frenkel defects are more stable.[63 64]

The substitutional doping of Cr_2O_3 with Ti^{4+} replacing a Cr^{3+} lattice site is assumed to be a HVD process with Cr vacancies forming to compensate the dopant.[27, 65] The process is expected to improve n-type conductivity from the excess electrons, however oxidation of the material occurs with the system exhibiting p-type conductivity,[65] as expected with LVD of chromia like Mg-Cr_2O_3.[56] This behavior is in contrast to the isostructural Fe_2O_3 system, where Ti doping displays n-type conductivity arising from an enhancement in free electron carrier concentration and mobility.[66, 67] Low Ti doping concentrations increase the n-type carrier concentration under oxygen poor conditions donating electrons to the conduction band by a polaron hopping mechanism. Under oxygen rich conditions Fe vacancies (V_{Fe}'''') are the main defect compensation process.[68]

There is some debate over the origin of conductivity in Ti doped Cr_2O_3, whether it is n-type or p-type under different oxygen conditions (high/low). The question of the Ti dopant oxidation state, either +3 or +4, will clearly impact on the nature of the proposed mechanisms.[69-74] A recent study combining x-ray photoelectron spectroscopy, x-ray adsorption near-edge spectroscopy and density functional theory calculations by Kaspar *et al.*[75] found that Ti^{4+} is present replacing a Cr^{3+} site by comparing structural disorder between theory and experiment, and Cr vacancies are the dominant defect at high Ti^{4+} concentrations that are present from a

Accepted Manuscript

compensation mechanism. At low Ti concentrations, oxygen interstitials are the proposed compensating defects, and this study showed that the presence of these compensating defects can resolve the nature of n-/p- type conductivity in Ti doped Cr_2O_3. The authors however assume that Ti^{4+} is present at all O_2 partial pressures and that either Cr vacancies/O interstitials are formed without consideration of other dominant defects such as oxygen vacancies, as explored for undoped and Mg doped chromia.[57] This ambiguity with Ti doping in chromia and its effect on the electronic structure, as well as defect formation requires further insights from theory. In particular oxygen vacancy formation is of interest in promoting the reducibility of chromia. To our knowledge, Ti is the most examined HVD dopant in chromia, and it is interesting to examine other HVDs in chromia to explore in a broader sense charge compensating mechanisms, oxygen vacancy formation and their effect on the electronic structure of chromia.

Density functional theory calculations with a Hubbard +U correction (DFT+U) applied to the Cr 3d and O 2p states are used to investigation cation and anion vacancy formation in a select number of HVD (M = Ti, Ce, V, Zr) in Cr_2O_3. Ti, Ce and V can have +3 (M_2O_3) and +4 (MO_2) oxidation states, indicating that they could be present as either in bulk Cr_2O_3, while Zr is a non-reducible oxide with only one stable oxidation state of +4 (ZrO_2). Our calculations indicate that Ti, Ce and V have +3 oxidation states for single metal doping of Cr_2O_3, and their +3 oxidation state are maintained when increasing to three metal dopants. However, spontaneous formation of Cr vacancies occurs by a charge compensating process for the three metal doped structures, oxidising the three M^{+3} dopants to M^{4+} by a non-classical compensation mechanism.

For Zr doping in Cr_2O_3, the classical mechanism for a +4 HVD occurs, as the Zr^{4+} atom reduces neighbouring Cr^{3+} to Cr^{2+} cations. The charge compensating Cr vacancy reoxidises the lattice Cr^{2+} species to Cr^{3+} providing the neutral charge ground state. Once the charge

Accepted Manuscript

neutral ground state for each doped structure is established, the formation energies for cation and anion vacancies is investigated. We show that for one metal dopant as an example of the incorrect electronic ground state, cation vacancy formation is promoted while supressing anion vacancies compared to the undoped structure; however once the correct charge neutral ground state is established by the defect structure $[3M_{Cr}^{\cdot} + V_{Cr}^{'''}]$, then the vacancy mechanism is altered to favour the formation of anion over cation vacancies to facilitate electron injection into the lattice.

2. Methodology

All calculations were performed using density functional theory (DFT) with the generalised gradient approximation (GGA)[76] and the Perdew Burke Ernzerhof (PBE)[77] exchange correlation functional as implemented in the Vienna *ab initio* Simulation Package (VASP).[78-80] The valence electrons are expanded by a plane wave basis set and the electronic interactions between the core (Cr:[Ar], O:[He], Ce:[Xe4], Ti:[Ar], V:[Ar], Zr:[Kr]) and valence (Cr $3d^5$ $4s^1$, O $2s^2$ $2p^4$, Ce $4f^1$ $5d^1$ $6s^2$, Ti $3p^6$ $3d^2$ $4s^2$, V $3p^6$ $3d^4$ $4s^1$, Zr $4s^2$ $4p^6$ $4d^2$ $5s^2$) electrons is described by the projected augmented wave method.[81, 82] To correctly describe the on-site coulombic interactions of the highly correlated valence electrons in each doped system, a Hubbard +U correction[83, 84] of U=+5eV and U=+5.5eV is applied to the Cr 3d and O 2p states,[6, 64] as well a +U=5eV for the Ce 4f,[40, 41] and +U=4.5eV for the Ti and V 3d.[34, 35, 85]

The optimisation of the Cr_2O_3 bulk was carried out at a series of constant volume calculations between ±0.2% of the experimental lattice constant were the atom positions, cell vectors, and angles were allowed to relax. These were tested at different plane wave cut-off energies and *k*-point sampling grids as described previously.[64] The structures were deemed converged when the forces on all ions were below 0.02 eV/Å^3 and the electronic convergence was $1x10^{-8}$

Accepted Manuscript

eV. The energies for each volume was fitted to the Murnaghan equation of state[86] which alleviates issues associated with Pulay stress. The parameters used for all bulk calculations were a plane wave energy cut off of 500eV and a Monkhorst-Pack[87] k-point sampling grid of 4x4x4. The minimum energy structure was found to deviate from the experimental structure by 2.48%[4], with a = b = 5.084 Å and c = 13.94 Å. With these technical parameters, the computed formation energy of bulk Cr_2O_3 is 2.75 eV / atom, which compares with the experimental value of 2.38 eV / atom[88].

The Cr_2O_3 bulk lattice was expanded to a (2x2x2) supercell with composition $Cr_{96}O_{144}$, which was converged using the computational set-up above, with a reduced k-point sampling grid of (2x2x2). To study doping of Cr_2O_3, a single metal dopant species (Ce, Ti, V, Zr) was substituted onto a Cr^{3+} cation site, to give a doping concentration of 1.04%. Chromium vacancy formation (Cr vac) was examined in metal doped system by removing all symmetry equivalent Cr cations around the dopant cation in nearest and next nearest neighbour positions. The formation energy for the Cr vacancy ($E[Cr^{vac}]$) is calculated from:

$$E[Cr^{vac}] = (E[MCr_{94}O_{144}] + yE[Cr_1]) - E[M{:}Cr_{95}O_{144}] \quad (6)$$

Where $E[M_x{:}Cr_{94}O_{144}]$ is the calculated energy of metal doped Cr_2O_3 containing a Cr vacancy, $E[Cr_1]$ is the reference energy of metallic Cr, and $E[M{:}Cr_{95}O_{144}]$ is the calculated energy for metal doped Cr_2O_3 with no Cr vacancy. The position of the most stable oxygen vacancy (O^{vac}) was explored in the same approach and the oxygen vacancy formation energy (E[O vac]) was calculated from:

$$E[O^{vac}] = (E[M{:}Cr_{95}O_{143}] + \tfrac{1}{2} E[O_2]) - E[M{:}Cr_{95}O_{144}] \quad (7)$$

Where $E[M{:}Cr_{95}O_{143}]$ is the calculated energy for the metal doped bulk containing an O vacancy, and $E[O_2]$ is the calculated energy of gaseous O_2 in a vacuum with a Hubbard +U correction of +U=5.5eV applied to the O 2p states.

Accepted Manuscript

The different oxidation states of the metal cations compared to the host Cr oxidation state means that we have to consider how to charge balance these oxidation state differences. If the metal dopants have a +4 oxidation state in Cr_2O_3, they can donate an electron to the host oxide to reduce a Cr^{3+} cation (equation 3), or a combination of three substitutional metal dopants is charge compensated by the spontaneous formation of a Cr vacancy, giving a $[3M_{\dot{C}r} + V_{Cr}^{'''}]$ defect. This then gives the correct electronic ground state for higher valence doping in Cr_2O_3. To determine the lowest energy configuration for three metal dopants, a range of Cr lattice sites were replaced by a dopant in nearest and next nearest neighbour sites relative to the single metal dopant to find the lowest energy arrangement of two dopants species in the Cr_2O_3 bulk (see structures and relative energies in the supporting information Figures S1 – S4). From the lowest energy distribution of two dopants, a third metal dopant is explored similarly to find the lowest energy arrangement for three metal dopants in the Cr_2O_3 lattice (see structures and relative energies in the supporting information Figures S5 – S8), at a dopant concentration of 3.125%. The compensation mechanism by Cr vacancy formation is explored by examining the removal of different Cr cations in nearest and next nearest neighbour sites. Upon finding the structure with the most stable arrangement of the three metal dopants and compensating Cr vacancies, $[3M_{\dot{C}r} + V_{Cr}^{'''}]$, this is used as the correct ground state structure to explore cation and anion vacancy formation. The calculation of the formation energies for the Cr and O vacancies in the charge compensated structures follow equations 6 and 7. The effect of the dopant on these defects is compared to the undoped Cr_2O_3 bulk and the single metal doped structures.

Accepted Manuscript

3. Results:

3.1 Chromium and oxygen vacancy formation in metal doped Cr_2O_3

A discussion on the detailed geometric and electronic structures, and energetics of vacancy formation for the undoped Cr_2O_3 lattice is presented in the supporting information, figures S9 – S10. For reference the computed Bader charges on Cr^{3+} cations and O^{2-} anions are 4.0 electrons (e^-) and 7.3 e^-. The number of valence electrons on Cr is 6 and on oxygen 6 electrons, giving net Bader charges of +2 and -1.7 electrons. We prefer to quote the computed Bader charge for cations and ions in this paper and will give the number of valence electrons where Bader charges are first quoted. The computed spin magnetisations are 3.0 μB and 0.0 μB for Cr^{3+} and O^{2-} species.

The calculated local structures for the single Ce, V, Ti and Zr dopants in bulk Cr_2O_3 along with the geometric and electronic information are shown in the supporting information figures S11 – S17. We note that the oxidation states of Cr and the dopants with one metal dopant in bulk Cr_2O_3 are +3 for Ce, V, Ti and Cr, with computed Bader charges of 9.9 e^-, 11.0 e^-, 9.9 e^- and 4.0 e^-, while the computed spin magnetisations are 0.98 μB, 1.92 μB, 0.89 μB and 3.0 μB; the valence charges are 12, 11 and 10 electrons for Ce, V and Ti. For Zr doping the oxidation states are +4 and +2 for Zr and Cr, with computed Bader charges of 9.4 e^- (12 valence electrons from Zr) and 4.6 e^-. The computed spin magnetisations are 0.03 μB and 3.7 μB.

Chromium vacancy formation in Ce, Ti, V and Zr doped Cr_2O_3 was explored by examining a number of Cr lattice sites in nearest, next nearest and next next nearest neighbour positions relative to the dopant cation. The calculated formation energy for the most stable Cr vacancy site in each of the doped structures are given in Table 1. Each of the dopants greatly lowers the formation energy for Cr vacancies in Cr_2O_3. Ce and Ti show similar formation energies,

Accepted Manuscript

while V has the highest formation energy and Zr doping has the lowest formation energy. The geometric and electronic structures for the lowest energy Cr vacancy in each of the doped structures is presented in the supporting information. There is a deficit of three electrons after formation of the Ce vacancy. The oxygen holes (denoted O^-) so formed have a computed Bader charge of 7.0 e^- and a spin magnetisation value of 0.7 μB, typical of such defects in metal oxides[35, 40, 41, 48, 64]. As Figure S13 shows, only two oxygen holes are formed in each of the doped Cr_2O_3 structure while it would be expected that three oxygen holes form. On closer inspection, the Ce, Ti and V dopants cation are in fact oxidised from M^{3+} to M^{4+} with calculated Bader charges of 9.6 e^-, 9.6 e^- and 10.8 e^-, respectively. The calculated spin magnetisation values for the Ce, Ti and V dopants is 0.0 μB, 0.0 μB, and 1.0 μB, further supporting the M^{4+} oxidation state. A different mechanism is seen in the Zr-Cr_2O_3 lattice, as the previously reduced Cr^{2+} cation in Zr-Cr_2O_3 is oxidised to Cr^{3+}, with a calculated Bader charge of 4.0 e^- and a calculated spin magnetisation value of 3.0 μB.

Table 1: The calculated formation energy for chromium vacancies (E_f [Cr vac]), and oxygen vacancies (E_f[O vac]) in single metal atom, M, doped (M= Ce, Ti, V, Zr) Cr_2O_3.

	E_f [Cr vac] (eV)	E_f [Ovac] (eV)
Cr_2O_3	4.59	4.11
Ce – Cr_2O_3	2.60	3.89
Ti – Cr_2O_3	2.56	4.09
V – Cr_2O_3	3.65	4.45
Zr – Cr_2O_3	1.70	3.50

Accepted Manuscript

Oxygen vacancy formation is explored in a similar manner to Cr vacancy formation by considering all oxygen sites around the dopant site. The calculated formation energies for the most stable oxygen vacancy position in doped Cr_2O_3 are shown in Table 1. Ce and Zr doping decrease the oxygen formation energy compared to undoped Cr_2O_3, with Zr having the lowest O vacancy formation energy. Ti doping has a similar O vacancy formation energy to the undoped Cr_2O_3 bulk, while V doping increases the oxygen vacancy formation energy in Cr_2O_3. The calculated O vacancy energies indicate that Ce and Zr doping will improve the reducibility of Cr_2O_3 while Ti and V will not.

Oxygen vacancy formation releases two electrons into Cr_2O_3, reducing two Cr^{3+} cations to Cr^{2+} cations (Figure S15). The reduced Cr^{2+} cations have computed Bader charges of 4.5 e^- and a computed spin magnetisation value of 3.7 μB. The Ce, Ti and V dopants maintain their M^{3+} oxidation state (calculated Bader charges of 9.9 e^-, 9.9 e^- and 11.2 e^- and spin magnetisations of 1 μB, 1 μB and 2 μB, respectively). The Zr dopant maintains its M^{4+} oxidation state with a calculated Bader charge of 9.4 e^- and a spin of 0 μB. In Zr-Cr_2O_3 three reduced Cr cations are present from a combination of the Zr HVD and the oxygen vacancy.

The calculated O vacancy formation energies are generally larger than the Cr vacancy energies as the hole formation from the Cr vacancy to oxidise the dopants and lattice O is a more favourable process than reducing lattice Cr cations by electron release from the O vacancy. The geometric and electronic structures for the lowest energy O vacancy in each of the doped structures is presented in the supporting information.

3.2 Charge compensation, chromium vacancy formation and oxygen vacancy formation in three metal doped Cr_2O_3

Accepted Manuscript

Higher valence dopants with a +4 oxidation state in Cr_2O_3 are expected to donate one electron into the system, and three dopants will donate three electrons. These electrons can be charge compensated by the spontaneous formation of Cr vacancies giving the neutral defect pair $[3M_{Cr}^{\cdot} + V_{Cr}^{'''}]$. This provides the charge compensated ground state electronic structure for the investigation of Cr and O vacancy formation.

The most stable structures for three Ce, Ti, V and Zr dopants in Cr_2O_3 are shown in Figure 1. The three Ce dopants prefer to be nearest neighbour to one another, with two dopants in the same Cr layer and the third dopant in the next Cr layer below. For three Ti dopants, the preferential arrangement of Ti atoms is in three consecutive Cr layers. When three V atoms are doped into Cr_2O_3, two V atoms prefer to be nearest neighbour to each other in the same Cr layer with the third atom in the next nearest Cr layer above the two atoms. The three Zr dopants are distributed over three different Cr layers. The metal dopants maintain their distorted octahedral geometries with similar calculated dopant -oxygen bond distances as the single metal dopant (see supporting information Table S1).

The computed Bader charges for the dopants are 9.8 e^- (x2) and 9.7 e^- for Ce, 9.9 e^- (x3) for Ti, 11.0 e^- (x3) for V, and 9.4 e^- (x3) for Zr. The calculated spin magnetisations for each dopant are 1.0 μB (x2) and 0.9 μB for Ce, 0.89 μB (x3) for Ti, 1.9 μB (x3) for V, and 0.0 μB (x3) for Zr. The calculated Bader charges and spin magnetisations indicate that the three metal dopants maintain a similar oxidation state as single metal doping; the three metals Ce, V and Ti have an oxidation state of M^{3+}, each Zr dopant has an M^{4+} oxidation state. The Cr cations have computed Bader charges and spin magnetisations similar to those for a single metal dopant.

The calculated PEDOS plots for three metal dopants in doped Cr_2O_3 are shown in Figure 2. The presence of Ce, Ti and V occupied defect peaks in the valence to conduction band region

Accepted Manuscript

is characteristic of their M^{3+} oxidation state. The absence of a Zr-derived defect peak in Zr-doped Cr_2O_3 indicates that the Zr dopants have an M^{4+} oxidation state. Since the Zr dopants have a higher oxidation state than Cr, this means that three electrons (one per Zr dopants) are donated to the Cr cations in Cr_2O_3, reducing three Cr cations to Cr^{2+}. These reduced Cr cations have calculated Bader charges of 4.5 e^- and spin magnetisations of 3.7 μB. The associated PEDOS plots of these reduced Cr cations are shown in the bottom panel of Figure 2(d) and they show the presence of occupied Cr 3d peaks in the band gap supporting the assignment of Cr^{2+} oxidation state from the Bader charges and spin magnetisation values.

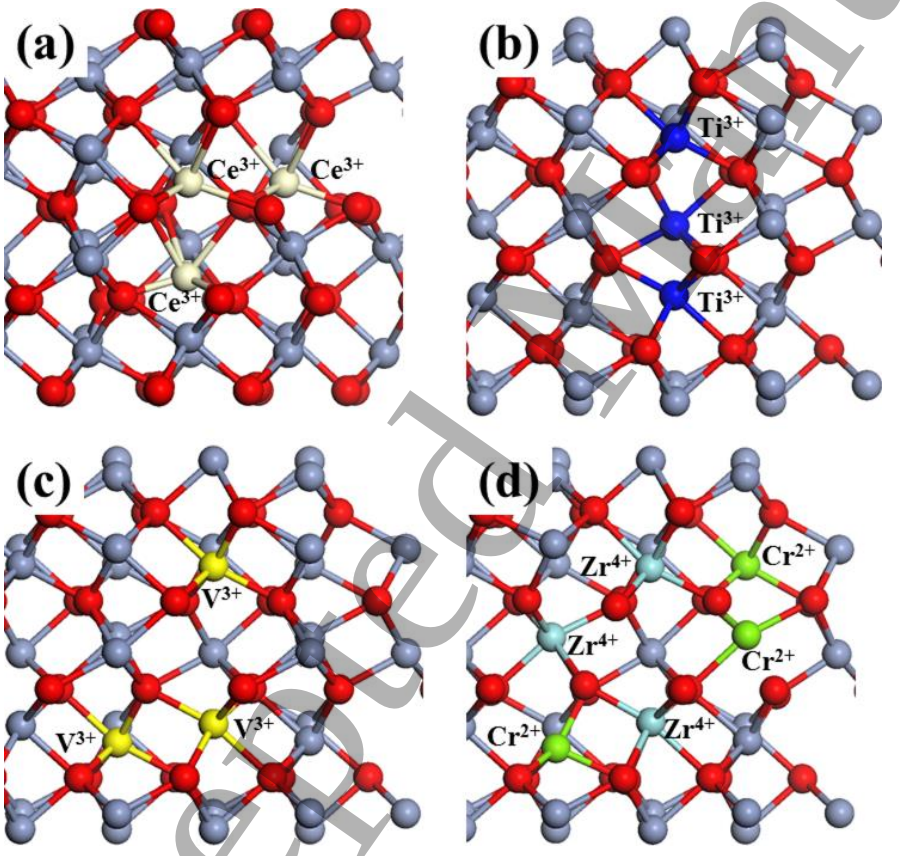


Figure 1: The calculated local structure for the lowest energy arrangement of three (a) Ce, (b) Ti, (c) V and (d) Zr in Cr_2O_3. The grey and red spheres are the lattice positions of the Cr and O atoms, while the white, dark grey and turquoise spheres are the lattice positions of the Ce, Ti/V and Zr dopants. The light green spheres are the positions of the reduced Cr cations.

Accepted Manuscript

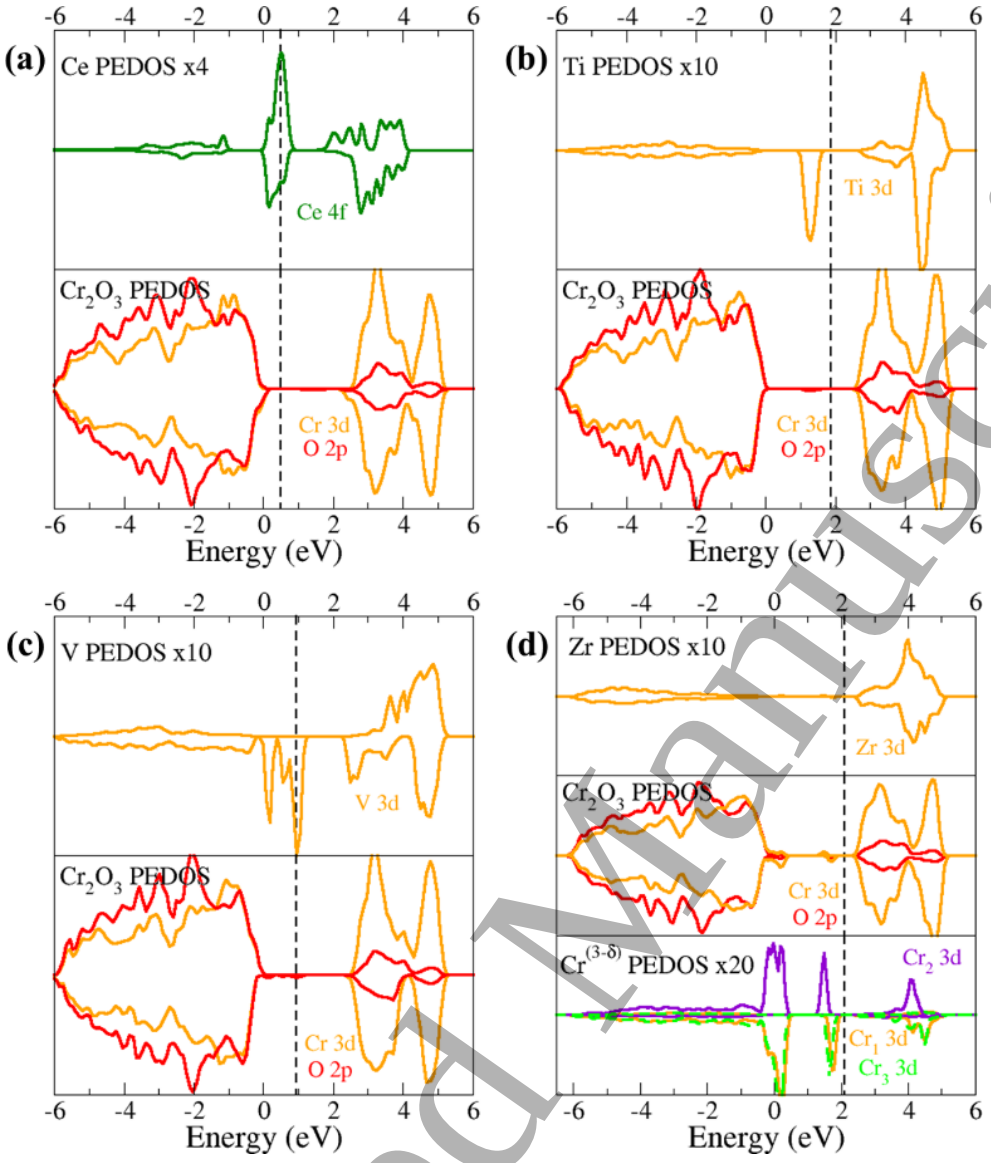


Figure 2: The calculated PEDOS plots for three (a) Ce, (b) Ti, (c) V and (d) Zr doped Cr_2O_3. The red, orange and green lines are the p, d and f states while the purple and light green lines are the reduced Cr 3d states. The top of the valence band is aligned to 0 eV and the black dotted line shows the position of the Fermi level

3.3 Charge Compensation via Chromium Vacancy Formation

Charge compensating mechanisms are important in a wide range of applications such as SOFC,[92, 93] and understanding their mechanism is important. The difference in oxidation state

Accepted Manuscript

between the metal dopants and the host Cr cations is compensated by formation of a Cr vacancy. Each Cr vacancy produces three holes which compensate the three electrons introduced by three dopants. The calculated formation energies for the most stable charge compensating Cr vacancy sites in doped Cr_2O_3 are given in Table 3. The negative formation energies for Ce, Ti and Zr doped Cr_2O_3 indicate that the Cr vacancy will form spontaneously and charge compensate the dopant. We note that for V doping that although the Cr vacancy formation energy is positive, it is rather low compared to Cr vacancy formation in undoped Cr_2O_3, which suggests that charge compensation also takes place. We confirm this by a hybrid DFT calculation using the screened hydrid Heyd-Scuseria-Ernzerhof (HSE06, 25 % HF exchange, screening length of 10 Å) exchange-correlation functional for which the computed Cr vacancy formation energy is -1.35eV. The negative formation energies for these charge compensating vacancies have also been found in DFT calculations of charge compensation in other metal oxides and hybrid DFT tends to yield more negative formation energies than DFT+U [35, 40, 41, 48, 64]

Table 3: Computed formation energies (PBE+U) for the charge compensating Cr vacancy in metal doped Cr_2O_3 (with three metal dopants).

	E_f [Cr comp] (eV)
3Ce – Cr_2O_3	-0.18
3Ti – Cr_2O_3	-0.64
3V – Cr_2O_3	+0.81
3Zr – Cr_2O_3	-2.02

Accepted Manuscript

The position of the lowest energy charge compensating Cr vacancy in each doped structure is shown in Figure 3. For Ce doping, the preferential position of the charge compensating Cr vacancy is nearest neighbour to the three Ce dopants and in the same Cr layer as two of the Ce dopants. This allows relaxation of the local atomic structure around the Ce dopant sites, which is important as Ce has a larger ionic radius than Cr. The lowest energy position of the charge compensating Cr vacancy is similar in Ti-Cr_2O_3 and Zr-Cr_2O_3. This site is in a nearest neighbour position to the three metal dopants and in the same cation layer as one of the dopant sites. For V doping, the stable Cr vacancy site lies in in the Cr layer between the pair of V dopants and the single V dopant.

The calculated Bader charges for the metal dopants after charge compensation are; 9.6 electrons (x3) for Ce, 9.6 electrons (x 3) for Ti, 10.8 electrons (x3) for V and 9.4 electrons (x3) for Zr. The calculated dopant spin magnetisations are 0 for Ce, Ti and Zr and the V dopants each have calculated spin magnetisations of 1.1 μB. For charge compensated Zr-Cr_2O_3, the previously reduced Cr cations are now reoxidised and the Bader charges are similar to those for oxidised Cr^{3+} cations in Cr_2O_3. These results for the charge compensated doped Cr_2O_3 systems indicate that a non-classical charge compensation mechanism takes place. The Cr vacancies oxidises the originally +3 Ce, Ti and V dopants to +4 cations. For 3Zr-Cr_2O_3, the traditional charge compensating mechanism by the Cr vacancy oxidises the reduced Cr lattice cations back to Cr^{3+} takes place. We relate this to the reducibility of Ce, Ti and V which means that a +3 oxidation state is stable for each dopant.

Accepted Manuscript

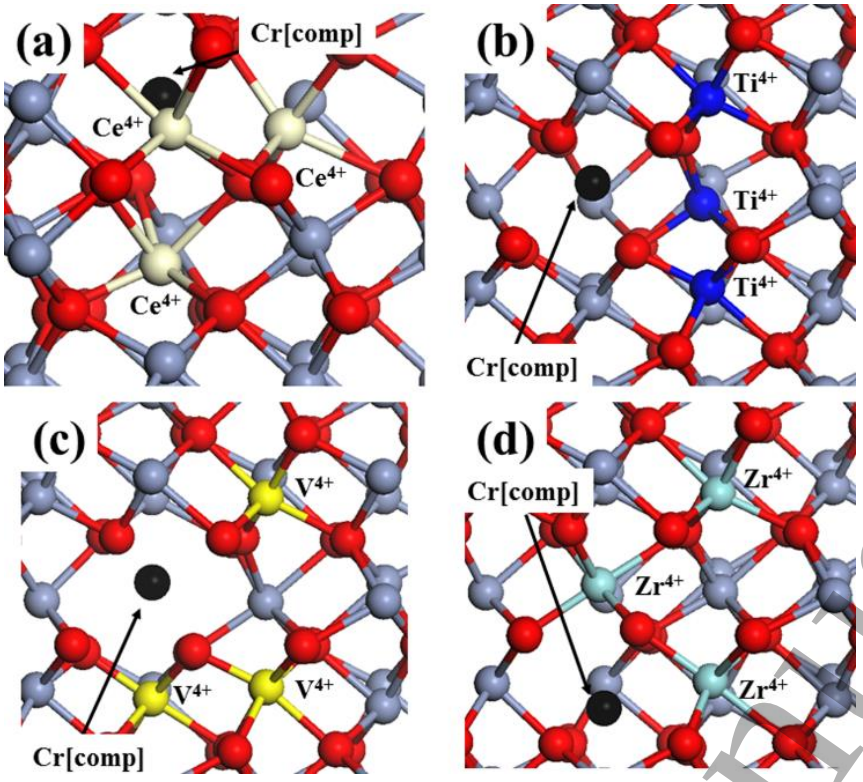


Figure 3: The calculated local structures for the lowest energy position of the Cr charge compensating vacancy in three metal (a) Ce, (b) Ti, (c) V, and (d) Zr doped Cr_2O_3. The grey and red spheres are the lattice positions of the Cr and O atoms, while the white, dark grey and turquoise spheres are the lattice positions of the Ce, Ti/V and Zr dopants. The black sphere is the position of the charge compensating Cr vacancy.

The calculated PEDOS plots for charge compensated doped Cr_2O_3 are shown in Figure 4. The absence of dopant derived occupied defect peaks in the band gap in the charge compensated structures indicates that the metals dopants exist in an oxidised +4 oxidation state for Ce, Ti and V doping. For Zr-Cr_2O_3, the previous Cr 3d occupied defect peaks in the band gap also disappear, which further supports the mechanism of reduction of Cr lattice cations to the +3 oxidation state. The absence of defect peaks in all systems indicates that these doped systems are indeed charge neutral and we now turn to investigating cation and anion vacancy formation.

Accepted Manuscript

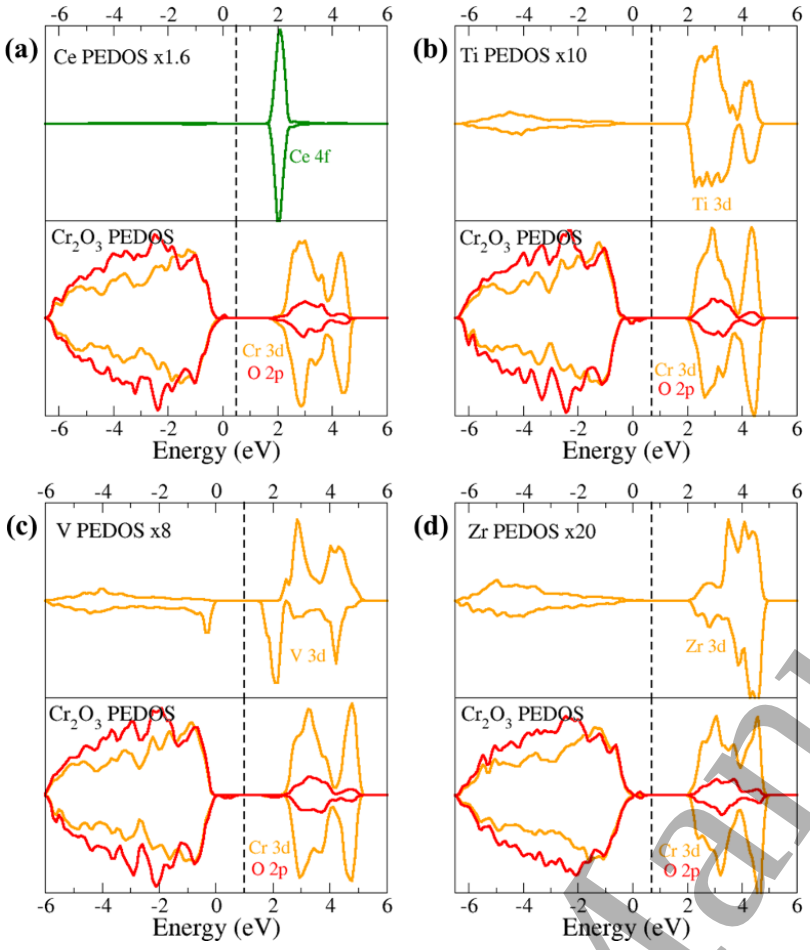


Figure 4: The calculated PEDOS plots for the three metal doped structures with the Cr charge compensated vacancy for (a) Ce, (b) Ti, (c) V and (d) Zr doped Cr_2O_3. The red, orange and green lines are the p, d and f states. The top of the valence band is aligned to 0 eV and the black dotted line shows the position of the Fermi level

3.4 Chromium vacancy and reducing oxygen vacancy formation

The removal of a second Cr vacancy from charge compensated doped Cr_2O_3 results in formation of the oxidising Cr vacancy. The calculated formation energies for the lowest energy configuration for the most stable oxidising Cr vacancy in each doped structure are given in Table 4. From the calculated formation energies, we can see that while Ce, Ti and Zr

Accepted Manuscript

doping promote Cr vacancy formation over Cr_2O_3 in the sense of lowering the formation energy relative to undoped Cr_2O_3, the energy cost is still rather larger, being 3.34 eV for the most favourable Ti-Cr_2O_3 system. V doping actually *increases* the formation energy of the oxidising Cr vacancy.

Table 4: The calculated formation energies for the Cr vacancy in the three metal doped Cr_2O_3 bulks.

	E_f [Cr vac] (eV)
Cr_2O_3	4.59
3Ce – Cr_2O_3	3.62
3Ti – Cr_2O_3	3.34
3V – Cr_2O_3	4.81
3Zr – Cr_2O_3	3.30

The lowest energy positions for the most stable Cr vacancy are shown in Figure 5. The position of the Cr vacancy is next nearest neighbour to the dopants and forms in the same Cr layer as the charge compensating Cr vacancy in Ce-, Ti- and V-doped Cr_2O_3. With Zr, the Cr vacancy forms in the next-next nearest neighbour positions to the three Zr dopants and in the Cr layer above the Cr compensated vacancy. All dopants are found to maintain their geometries as in the doped structures with similar bond lengths. From calculated Bader and spin magnetisation values, the dopants maintain their +4 oxidation states with similar Bader charges and spin magnetisations as the charge compensated structures. In structure, the Cr vacancy forms three holes on nearest neighbour O atoms. These are identified by calculated

Accepted Manuscript

Bader charges and spin magnetisation of 7.0 e^- and 0.7 μB, respectively. These value are typical of localised oxygen holes from these DFT+U computations[35, 40, 41, 48, 64].

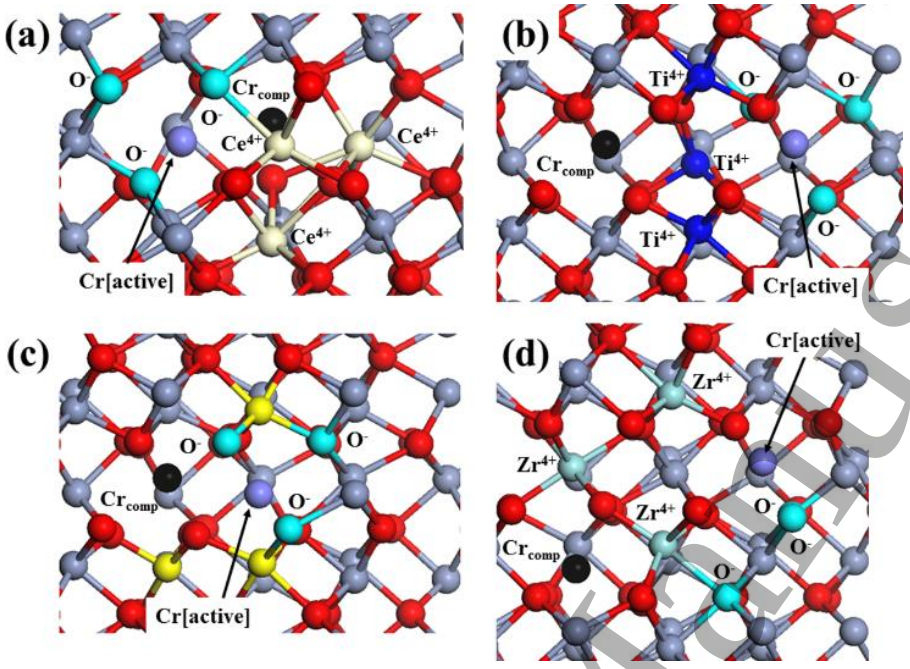


Figure 5: The calculated local geometries for the lowest energy position for the active Cr vacancy in (a) Ce, (b) Ti, (c) V and (d) Zr doped Cr_2O_3. The grey and red spheres are the lattice positions of the Cr and O atoms, while the white, blue, yellow and turquoise spheres are the lattice positions of the Ce, Ti, V and Zr dopants. The black sphere is the position of the charge compensating Cr vacancy, the purple sphere is the Cr vacancy, and the light blue spheres are the O^- species.

The calculated PEDOS plots after Cr vacancy formation are given in Figure 6. The lack of dopant electrons states in the band gap confirms that the dopants are in a +4 oxidation state and the major contributions of the dopants are to the CB states. The lower panel of the PEDOS plots show the PEDOS of the O^- lattice species for which three unoccupied O 2p peaks are visible between 0.8 – 1.2 eV above the VB. These states are characteristic of hole states on the lattice O atoms.

Accepted Manuscript

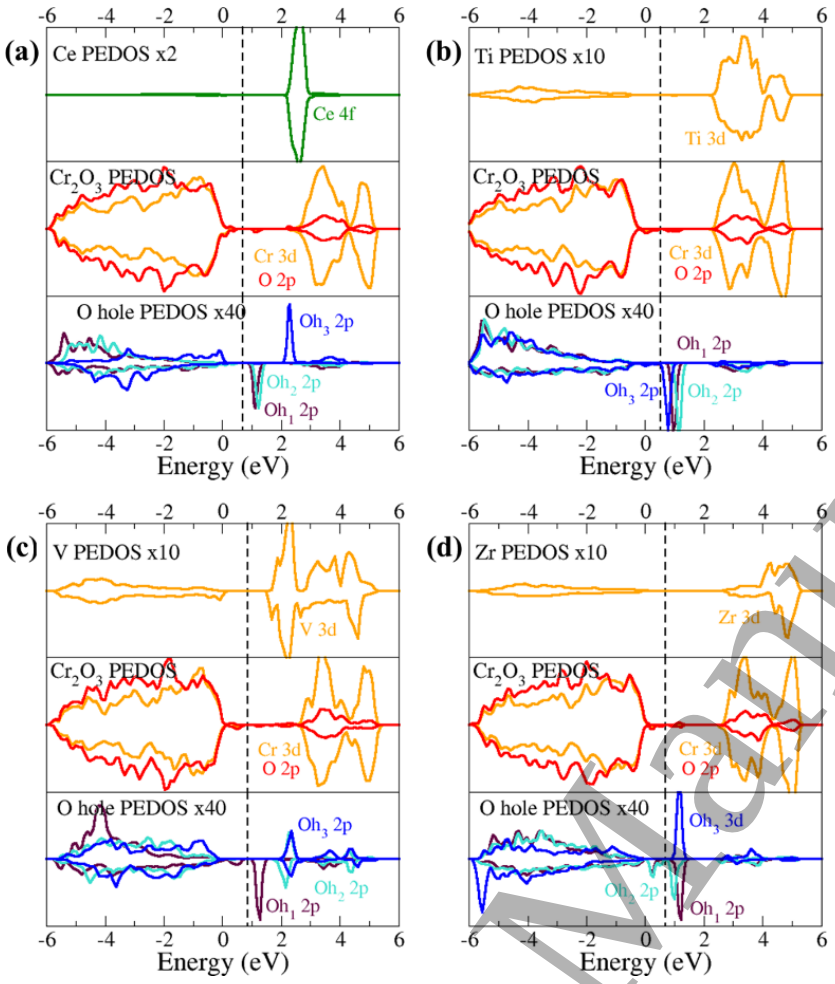


Figure 6: The calculated PEDOS plots for the active Cr vacancy for (a) Ce, (b) Ti, (c) V and (d) Zr doped Cr_2O_3. The red, orange and green lines are the p, d and f states. The light blue, dark blue and maroon lines in the lowest panel on the plot are the O 2p states for the O^- species. The top of the valence band is aligned to 0 eV and the black dotted line shows the position of the Fermi level.

The formation of the reducing oxygen vacancy in doped bulk Cr_2O_3 was investigated by trialling all possible inequivalent lattice oxygen lattice sites to determine the site of the lowest energy vacancy site. The calculated formation energies for most stable reducing oxygen vacancy in each doped structure are given in Table 5. All dopants decrease the formation energy of reducing oxygen vacancies compared to undoped Cr_2O_3 indicating that HVDs

Accepted Manuscript

could enhance the reducibility of Cr_2O_3. Ce shows the greatest enhancement in oxygen vacancy formation in doped Cr_2O_3, while V shows the smallest effect. These energies indicate that Ce is the higher valent dopant of choice to improve the reducibility of Cr_2O_3. We propose that this arises from the larger ionic radius of Ce^{3+} that can distort the local geometry, as also discussed for alkali doped Cr_2O_3[89].

Table 5: The calculated formation energies for the oxygen vacancy in three metal doped Cr_2O_3.

	E_f [O vac] (eV)
Cr_2O_3	4.11
3Ce – Cr_2O_3	2.83
3Ti – Cr_2O_3	3.04
3V – Cr_2O_3	3.83
3Zr – Cr_2O_3	3.14

The atomic structures for the most stable oxygen vacancy in each doped structure are shown in Figure 7. All dopant species have similar geometries, with similar M-O bond lengths as their local geometry in the charge compensated structures. The position of the most stable O vacancy is in the layer below that layer containing the charge compensating Cr vacancy for all dopants. The vacancy site is next nearest neighbour to the dopants in each structure. For Ti-, V-, and Zr-doped Cr_2O_3 structures, the calculated Bader charges and spin magnetisations indicate that the dopants maintain their +4 oxidation states with similar computed values to Cr vacancy compensated doped structures. The formation of an oxygen vacancy reduces two nearest neighbouring Cr lattice cations to Cr^{2+}, which now have computed Bader charges of

Accepted Manuscript

4.5 e^- and spin magnetisations of 3.7 µB. These Cr^{2+} cations have a four-coordinate square planar geometry, as shown in figure 7. For Ce doping, a different reduction mechanism is observed as the oxygen vacancy reduces a nearest neighbour Cr cation and one of the Ce dopants. The reduced Cr dopant has a calculated Bader charge of 4.5 e^- and a computed spin magnetisation of 3.7 µB, while the reduced Ce^{3+} dopant has a Bader charge of 9.9 e^- and a spin of 1 µB.

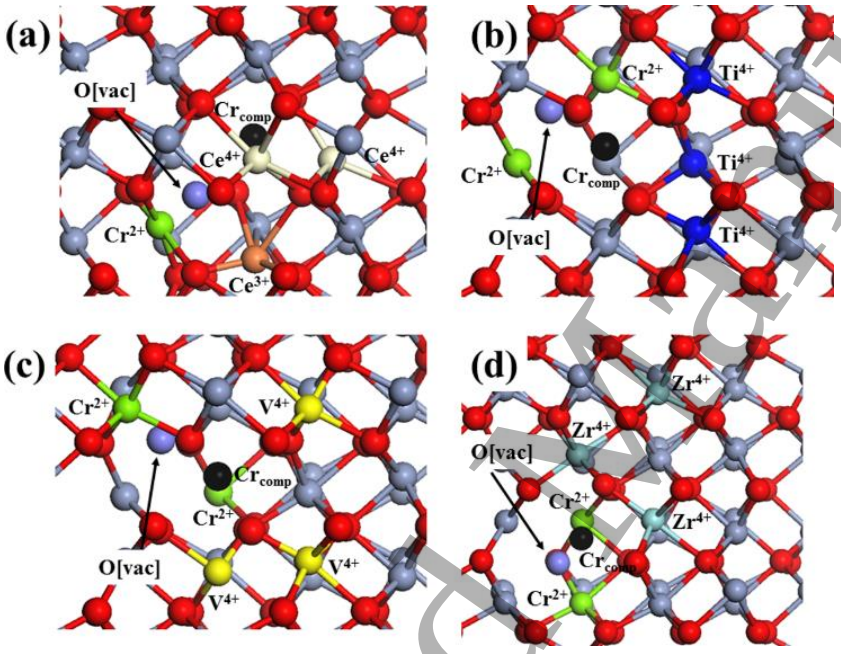


Figure 7: The calculated local geometries for the lowest energy position for the active O vacancy in (a) Ce, (b) Ti, (c) V and (d) Zr doped Cr_2O_3. The grey and red spheres are the lattice positions of the Cr and O atoms, while the white, blue, yellow and turquoise spheres are the lattice positions of the Ce, Ti, V and Zr dopants. The black sphere is the position of the charge compensating Cr vacancy, the purple sphere is the active O vacancy, and the light green spheres are the Cr^{2+} species.

The calculated PEDOS plots for the most stable oxygen vacancy structures for each dopant are shown in Figure 8. The reduction of one Ce dopant and one Cr cation in Ce-Cr_2O_3 is

Accepted Manuscript

further confirmed by the appearance of occupied Ce 4f and Cr 3d peaks around 1 eV above the top of the VB in the band gap, consistent with Cr^{3+} and Cr^{2+} species. For the Ti-, V-, and Zr-Cr_2O_3 structures, the reduction of the two Cr lattice cations to Cr^{2+} is indicated by the appearance of occupied Cr 3d defect peaks around 1eV above the top of the VB and no PEDOS peaks characteristic of reduced cations. In Ti- and V doped structures, these defect peaks have the same spin, while in 3Zr doped Cr_2O_3 the Cr 3d defect peaks have opposing spins.

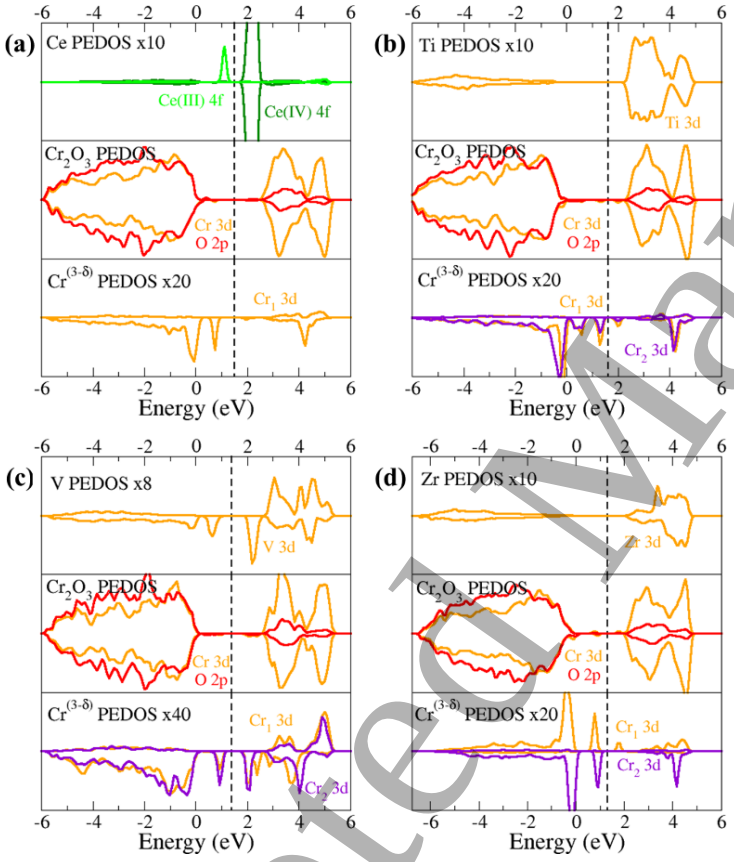


Figure 8: The calculated PEDOS plots for the O vacancy for (a) Ce, (b) Ti, (c) V and (d) Zr doped Cr_2O_3. The red, orange and green lines are the p, d and f states. The orange and purple lines in the lowest panel on the plot are the Cr 3d states for the Cr^{2+} species. The top of the valence band is aligned to 0 eV and the black dotted line shows the position of the Fermi level.

Accepted Manuscript

4 Discussion

The effect of higher valence doping of Cr_2O_3 with Ce, Ti, V and Zr on the electronic structure, cation oxidation states and cation/anion vacancy formation is investigated using DFT, within the PBE+U formalism. Upon incorporation onto a Cr lattice site, Ce, Ti, and V dopants have a +3 oxidation state, rather than the +4 oxidation state that may be expected by substituting into a reducible oxide. The reason for this is that these dopants can access multiple oxidation states, in particular the +3 oxidation state. By contrast, the Zr dopant has the +4 oxidation state that would be expected for a higher valence dopant and one Cr cation reduces to Cr^{2+}. Only this oxidation state is possible with non-reducible Zr..

For doping of one Cr lattice site in Cr_2O_3, giving a doping concentration of 1%, Cr vacancy formation is promoted and would be more favourable than O vacancy formation. The Cr vacancy formation is facilitated by the flexible oxidation state of Ce, Ti and V as they are oxidised to the +4 oxidation state after Cr vacancy formation. With Zr doped Cr_2O_3, the holes generated by the Cr vacancy oxidise a previously reduced lattice Cr^{2+} cation and this helps to lower the Cr vacancy formation energy compared to the other dopant species as Cr reoxidation is probably more favourable than the oxidation of the other metal dopants as indicated by the lower Cr vacancy formation energy (Table 1).

Upon increasing the concentration of dopants to 3 %, the Ce, Ti and V dopants maintain their +3 oxidation state, and the three Zr dopants in the lattice maintain their +4 oxidation state but reduce three neighbouring Cr cations. For all metal dopants with this concentration, a charge compensation mechanism occurs by spontaneous formation of a Cr vacancy. Different mechanisms are observed depending on whether the metal dopant has a variable or non-variable oxidation state. The charge compensation process for Zr doping follows the classical mechanism, by which the higher valence dopants reduce three lattice Cr cations which are then compensated by the generation of holes from the Cr vacancy to give the charge neutral

Accepted Manuscript

ground state electronic structure. This mechanism is not observed for the metal dopants with varying oxidation states, where we see a non-classical mechanism as the formation of the Cr vacancy proceeds by charge compensation that oxidises the metal dopants from M^{+3} to M^{+4}.

Once the correct ground state electronic structures for the doped systems has been established, the calculated formation energies for Cr and O vacancies show that O vacancy formation is favoured over Cr vacancy formation in all doped systems. The Ce, and Ti dopants promote oxygen vacancy formation to a greater extent than V and Zr since Ce and Ti are highly reducible oxides in their MO_2 structures. By contrast, doping at 1%, with a single metal atom without charge compensation promotes Cr vacancy formation.

The change in promoting vacancy formation from Cr vacancies in the single metal doped system to O vacancies for a higher concentration of metal dopants is caused by the different description of the ground state electronic structures. The single metal dopants have a +3 oxidation state for Ce, Ti and V, with a reduced Cr cation in the Zr doped system. The formation of the Cr vacancy tries to compensate these charges by oxidising the M^{3+} dopants to M^{+4} and Cr^{2+} to Cr^{3+} cation in Zr-Cr_2O_3, which may over stabilise the vacancy formation energy. For the three metal dopants with a Cr vacancy in Cr_2O_3, the structures are charge compensated, irrespective of the compensation mechanism and provide the correct electronic structure to investigate the cation and anion vacancy formation energies.

The non-classical behaviour of dopant charge compensation formation of a Cr vacancy was not considered in previous studies,[64-66,72,73] which have debated if Ti exists in a M^{3+} or M^{4+} oxidation state. The experimental studies have found that Ti is incorporated as an M^{4+} dopant species. We have shown whether we consider a low Ti concentration (single metal doped systems) or larger Ti concentration (three metal doped systems), Ti^{4+} will always for either by more facile Cr vacancy formation or Cr vacancy charge compensation and this will hold

Accepted Manuscript

for Ce and V dopants, which we propose will have a +4 oxidation state when doped into Cr_2O_3.

Doping with higher valence dopants is explored as an approach to inject electrons into the a metal oxide and it would be expected that a further electron donation process such as anion vacancy formation will not be favoured due to the presence of excess electrons. However, as we describe a charge neutral system that has formed by charge compensation, the correct defect process is therefore described and these higher valence dopants thus improve reducibility of bulk Cr_2O_3. The electron donation process therefore in metal doped Cr_2O_3 is by an oxygen vacancy mediated process, rather by electron donation from the dopant cations. In experimental systems, it is probable that the three metal doped cluster description in the bulk Cr_2O_3 lattice for this study is more likely to exist since doping concentrations are typically greater than 10% and the distribution of doped metal cations will resemble the Cr vacancy compensated structures.

The results of this study have implications in considering the doping mechanisms for higher valence doping in Cr_2O_3 for catalyst design and transport layers in energy harvesting materials. Cr_2O_3 cannot be a p-type semi-conductor, or a hole conducting layer by higher valence doping of these selected metal dopants. The non-classical behaviour of high valence metal doped Cr_2O_3 will trap holes generated by Cr vacancies by favouring a dopant 4+ oxidation state or a charge compensating mechanism by a Cr vacancy formation, which neutralise any holes that may be generated. Also, the classical mechanism for Zr doping will also trap holes by donation of electrons from the Zr dopant. The dopants will achieve charge neutrality and favour formation of oxygen vacancies which will then inject electrons into the bulk system that can combine and kill any other holes that may be present. The promotion of oxygen vacancy formation and increased reducibility of Cr_2O_3 by these dopants have useful

Accepted Manuscript

applications in oxygenation catalysis such as methanol synthesis, or electrolyte materials in solid oxide fuel cells.

5 Conclusion

Density functional theory (DFT) calculations using the Perdew-Burke-Ernzerhof (PBE) exchange correlation functional within the generalised gradient approximation (GGA), and the Hubbard +U correction (PBE+U) applied to the Cr 3d and O 2p states, were used to investigate higher valence doping of Ce, Ti, V and Zr in Cr_2O_3. Ce, Ti and V dopants are found to have a +3 oxidation state, while Zr metal has a +4 oxidation state in the Cr_2O_3 lattice. Cr vacancies generate holes in the lattice and oxidise the Ce, Ti, V dopants from M^{3+} to M^{4+} and also lattice O^{2-} to O^{-}, while for Zr doping the reduced lattice Cr cation and two lattice O are oxidised. All single metal dopants promote Cr vacancy over O vacancy formation, which is attributed to the over-binding of the charged atoms by the holes and the incorrect description of the ground state electronic structure. The bulk lattice with three metal dopants show that each of the metal dopants maintain their oxidation states similarly to the single metal systems, and a Cr vacancy compensated mechanism occurs in each of the doped Cr_2O_3 structures. For the Ce^{3+}, Ti^{3+} and V^{3+} a non-classical compensation mechanism is seen to happen where all three metals in the bulk lattice are oxidised to M^{4+} by spontaneous formation of a Cr vacancy. The charge compensating process in the non-reducible Zr cation doped Cr_2O_3 structure proceeds by a classical mechanism where the reduced lattice Cr cations by the Zr dopants are oxidised by the holes generated from the spontaneous Cr vacancy. This explains the experimental observations that Ti doped in Cr_2O_3 exists in a +4 oxidation state and predicts that both Ce and V will also be seen as +4 dopants in Cr_2O_3 by a similar mechanism. The charge compensated structures provide the correct ground state

Accepted Manuscript

electronic structure to investigate cation and anion vacancy formation. The compensated structures show that O vacancy formation is favoured over Cr vacancies, which is opposite to that observed for the single metal doped structures, providing further evidence that single metal doping with these dopants will provide an incorrect description of the electronic structure. These dopants thus increase the reducibility of Cr_2O_3 which have implications in rational design of catalysts and oxygen conducting layers in energy harvesting materials.

6 Acknowledgements:

We acknowledge support from the European Commission funded FP7-NMP project BIOGO (grant: 604296), the Science Foundation Ireland (SFI) and Higher Education Authority (HEA) funded Irish Centre for High-end Computing (ICHEC) and SFI funded local clusters at Tyndall, for computing resources. The COST ACTION CM1104 is thanked for support.

7 References:

1. K. J. W. Atkinson, R. W. Grimes, M. R. Levy, Z. L. Coull and T. English, *Journal of the European Ceramic Society*, 2003, 23, 3059-3070.
2. E. NEWNHAM and Y. D. HAAN, *Zeitschrift für Kristallographie-Crystalline Materials*, 1962, 117, 235-237.
3. N. Popovici, M. L. Paramês, R. C. Da Silva, O. Monnereau, P. M. Sousa, A. J. Silvestre and O. Conde, *Applied Physics A: Materials Science and Processing*, 2004, 79, 1409-1411.
4. R. K. Di Cerbo and A. U. Seybolt, *Journal of the American Ceramic Society*, 1959, 42, 430-431.
5. G. Rollmann, A. Rohrbach, P. Entel and J. Hafner, *Physical Review B*, 2004, 69, 165107.

Accepted Manuscript

6. A. Rohrbach, J. Hafner and G. Kresse, *Physical Review B*, 2004, 70, 125426.
7. L. M. Corliss, J. M. Hastings, R. Nathans and G. Shirane, *Journal of Applied Physics*, 1965, 36, 1099-1100.
8. P. J. Brown, J. B. Forsyth, E. Lelièvre-Berna and F. Tasset, *Journal of Physics: Condensed Matter*, 2002, 14, 1957.
9. R. Zimmermann, P. Steiner and S. Hüfner, in *Proc. 11th Intern. Conf. Vac. UV Rad. Phys.* , eds. T. Miyahara, Y. Azuma, M. Watanabe and T. Ishii, Elsevier, Amsterdam, 1996, DOI: http://dx.doi.org/10.1016/B978-0-444-82245-1.50016-9, pp. 49-52.
10. T. Uozumi, K. Okada and A. Kotani, *Journal of Electron Spectroscopy and Related Phenomena*, 1996, 78, 103-106.
11. T. Uozumi, K. Okada, A. Kotani, R. Zimmermann, P. Steiner, S. Hüfner, Y. Tezuka and S. Shin, *Journal of Electron Spectroscopy and Related Phenomena*, 1997, 83, 9-20.
12. O. Nakayama, N. Ikenaga, T. Miyake, E. Yagasaki and T. Suzuki, *Industrial and Engineering Chemistry Research*, 2010, 49, 526-534.
13. S. A. El-Molla, *Applied Catalysis A: General*, 2005, 280, 189-197.
14. E. M. Calverley and K. J. Smith, *Industrial and Engineering Chemistry Research*, 1992, 31, 792-803.
15. J. A. Cline, A. A. Rigos and T. A. Arias, *The Journal of Physical Chemistry B*, 2000, 104, 6195-6201.
16. M. P. Brady, B. A. Pint, Z. G. Lu, J. H. Zhu, C. E. Milliken, E. D. Kreidler, L. Miller, T. R. Armstrong and L. R. Walker, *Oxidation of Metals*, 2006, 65, 237-261.
17. E. C. Sara, W. Yong, L. Kenneth, C. K. Tiffany, W. C. Alicia, R. G. Daniel, G. Niranjan, V. S. Peter and A. C. Scott, *Journal of Physics: Condensed Matter*, 2013, 25, 392002.
18. H. Mashiko, T. Oshima and A. Ohtomo, *Applied Physics Letters*, 2011, 99, 241904.
19. T. C. Kaspar, D. K. Schreiber, S. R. Spurgeon, M. E. McBriarty, G. M. Carroll, D. R. Gamelin and S. A. Chambers, *Advanced Materials*, 2016, 28, 1616-1622.

Accepted Manuscript

20. A. Beretta, Q. Sun, R. G. Herman and K. Klier, *Industrial & engineering chemistry research*, 1996, 35, 1534-1542.
21. S. Mehta, G. W. Simmons, K. Klier and R. G. Herman, *Journal of Catalysis*, 1979, 57, 339-360.
22. Ø. Borck and E. Schröder, *Journal of Physics: Condensed Matter*, 2006, 18, 10751.
23. J. Hu, H. Li, X. Huang and L. Chen, *Solid State Ionics*, 2006, 177, 2791-2799.
24. R. F. Huang, A. K. Agarwal and H. U. Anderson, *Journal of the American Ceramic Society*, 1984, 67, 146-150.
25. N. Kohli, O. Singh and R. Singh, *Applied Physics A*, 2012, 109, 585-590.
26. P. T. Moseley and D. E. Williams, *Sensors and Actuators B: Chemical*, 1990, 1, 113-115.
27. G. S. Henshaw, D. H. Dawson and D. E. Williams, *Journal of Materials Chemistry*, 1995, 5, 1791-1800.
28. Y. Matsuzaki and I. Yasuda, *Journal of The Electrochemical Society*, 2001, 148, A126-A131.
29. X. Chen, P. Y. Hou, C. P. Jacobson, S. J. Visco and L. C. De Jonghe, *Solid State Ionics*, 2005, 176, 425-433.
30. Y. Liu and D. Chen, *international journal of hydrogen energy*, 2009, 34, 9220-9226.
31. M. Xiao, M. Zhao, X. Lang, Y. Zhu and Q. Jiang, *Chemical Physics Letters*, 2012, 542, 85-88.
32. M. Batzill, E. H. Morales and U. Diebold, *Physical review letters*, 2006, 96, 026103.
33. T. R. Gordon, M. Cargnello, T. Paik, F. Mangolini, R. T. Weber, P. Fornasiero and C. B. Murray, *Journal of the American Chemical Society*, 2012, 134, 6751-6761.
34. A. Iwaszuk and M. Nolan, *The Journal of Physical Chemistry C*, 2011, 115, 12995-13007.
35. A. Iwaszuk and M. Nolan, *Journal of Physics: Condensed Matter*, 2011, 23, 334207.

Accepted Manuscript

36. I. Nakamura, N. Negishi, S. Kutsuna, T. Ihara, S. Sugihara and K. Takeuchi, *Journal of Molecular Catalysis A: Chemical*, 2000, 161, 205-212.
37. R. Schaub, E. Wahlström, A. Rønnau, E. Lægsgaard, I. Stensgaard and F. Besenbacher, *Science*, 2003, 299, 377-379.
38. R. Schaub, P. Thostrup, N. Lopez, E. Lægsgaard, I. Stensgaard, J. K. Nørskov and F. Besenbacher, *Physical Review Letters*, 2001, 87, 266104.
39. L. Jing, B. Xin, F. Yuan, L. Xue, B. Wang and H. Fu, *The Journal of Physical Chemistry B*, 2006, 110, 17860-17865.
40. J. J. Carey and M. Nolan, *Applied Catalysis B: Environmental*, 2016, 197, 324-336.
41. J. J. Carey and M. Nolan, *Catalysis Science & Technology*, 2016, 6, 3544-3558.
42. P. Fornasiero, R. Dimonte, G. R. Rao, J. Kaspar, S. Meriani, A. Trovarelli and M. Graziani, *Journal of Catalysis*, 1995, 151, 168-177.
43. P. R. Keating, D. O. Scanlon and G. W. Watson, *Chemical Physics Letters*, 2014, 608, 239-243.
44. P. R. Keating, D. O. Scanlon and G. W. Watson, *Journal of Materials Chemistry C*, 2013, 1, 1093-1098.
45. P. R. Keating, D. O. Scanlon, B. J. Morgan, N. M. Galea and G. W. Watson, *The Journal of Physical Chemistry C*, 2012, 116, 2443-2452.
46. M. Nolan, S. C. Parker and G. W. Watson, *Surface Science*, 2005, 595, 223-232.
47. M. Nolan, J. E. Fearon and G. W. Watson, *Solid State Ionics*, 2006, 177, 3069-3074.
48. M. Nolan, *The Journal of Physical Chemistry C*, 2011, 115, 6671-6681.
49. M. Nolan, *Journal of Materials Chemistry*, 2011, 21, 9160-9168.
50. A. B. Kehoe, D. O. Scanlon and G. W. Watson, *Chemistry of Materials*, 2011, 23, 4464-4468.
51. P. Qin, G. Fang, N. Sun, X. Fan, Q. Zheng, F. Chen, J. Wan and X. Zhao, *Thin Solid Films*, 2011, 519, 4334-4341.

Accepted Manuscript

52. P. Qin, G. Fang, Q. He, N. Sun, X. Fan, Q. Zheng, F. Chen, J. Wan and X. Zhao, *Solar Energy Materials and Solar Cells*, 2011, 95, 1005-1010.
53. H. Cao, X. Qiu, Y. Liang, M. Zhao and Q. Zhu, *Applied Physics Letters*, 2006, 88, 241112.
54. E. Arca, K. Fleischer and I. V. Shvets, *Applied Physics Letters*, 2011, 99, 111910.
55. E. Arca, K. Fleischer, S. A. Krasnikov and I. Shvets, *The Journal of Physical Chemistry C*, 2013, 117, 21901-21907.
56. L. Farrell, K. Fleischer, D. Caffrey, D. Mullarkey, E. Norton and I. V. Shvets, *Physical Review B*, 2015, 91, 125202.
57. A. B. Kehoe, A. Elisabetta, D. O. Scanlon, I. V. Shvets and G. W. Watson, *Journal of Physics: Condensed Matter*, 2016, 28, 125501.
58. A. Holt and P. Kofstad, *Solid State Ionics*, 1997, 100, 201-209.
59. J. S. Park and H. G. Kim, *Journal of the American Ceramic Society*, 1988, 71, 173-176.
60. W. C. Hagel, *Journal of Applied Physics*, 1965, 36, 2586-2587.
61. Z. H. Zeng, M. Bjorketun, E., S. Ebbesen, M. Mogensen, B. and J. Rossmeisl, *Physical Chemistry Chemical Physics*, 2013, 15.
62. Z. Zeng, M. H. Hansen, J. P. Greeley, J. Rossmeisl and M. Bjorketun, E., *J. Phys. Chem. C*, 2014, 118.
63. F. Lebreau, M. M. Islam, B. Diawara and P. Marcus, *The Journal of Physical Chemistry C*, 2014, 118, 18133-18145.
64. J. J. Carey, M. Legesse and M. Nolan, *The Journal of Physical Chemistry C*, 2016, 120, 19160-19174.
65. D. Niemeyer, D. E. Williams, P. Smith, K. F. E. Pratt, B. Slater, C. R. A. Catlow and A. Marshall Stoneham, *Journal of Materials Chemistry*, 2002, 12, 667-675.
66. T. Droubay, K. M. Rosso, S. M. Heald, D. E. McCready, C. M. Wang and S. A. Chambers, *Physical Review B*, 2007, 75, 104412.
67. M. Rioult, H. Magnan, D. Stanescu and A. Barbier, *The Journal of Physical Chemistry C*, 2014, 118, 3007-3014.

Accepted Manuscript

68. B. Zhao, T. C. Kaspar, T. C. Droubay, J. McCloy, M. E. Bowden, V. Shutthanandan, S. M. Heald and S. A. Chambers, *Physical Review B*, 2011, 84, 245325.
69. A. Holt and P. Kofstad, *Solid State Ionics*, 1999, 117, 21-25.
70. A. Holt and P. Kofstad, *Solid State Ionics*, 1994, 69, 137-143.
71. A. Atkinson, M. R. Levy, S. Roche and R. A. Rudkin, *Solid State Ionics*, 2006, 177, 1767-1770.
72. A. Conde-Gallardo, A. Cruz-Orea, O. Zelaya-Angel and P. Bartolo-Pèrez, *Journal of Physics D: Applied Physics*, 2008, 41, 205407.
73. V.-T. Rangel-Kuoppa and A. Conde-Gallardo, *Thin Solid Films*, 2010, 519, 453-456.
74. F. Maldonado, C. Novillo and A. Stashans, *Chemical Physics*, 2012, 393, 148-152.
75. T. C. Kaspar, P. V. Sushko, M. E. Bowden, S. M. Heald, A. Papadogianni, C. Tschammer, O. Bierwagen and S. A. Chambers, *Physical Review B*, 2016, 94, 155409.
76. J. P. Perdew and W. Yue, *Physical review B*, 1986, 33, 8800.
77. J. P. Perdew, K. Burke and M. Ernzerhof, *Physical review letters*, 1996, 77, 3865.
78. G. Kresse and J. Furthmüller, *Computational Materials Science*, 1996, 6, 15-50.
79. G. Kresse and J. Furthmüller, *Physical Review B*, 1996, 54, 11169.
80. G. Kresse and J. Furthmüller, *Phys. Rev. B*, 1996, 54, 169.
81. G. Kresse and J. Hafner, *Journal of Physics: Condensed Matter*, 1994, 6, 8245.
82. G. Kresse and D. Joubert, *Physical Review B*, 1999, 59, 1758.
83. S. L. Dudarev, A. I. Liechtenstein, M. R. Castell, G. A. D. Briggs and A. P. Sutton, *Physical Review B*, 1997, 56, 4900-4908.
84. S. Dudarev, G. Botton, S. Savrasov, C. Humphreys and A. Sutton, *Physical Review B*, 1998, 57, 1505.
85. D. O. Scanlon, A. Walsh, B. J. Morgan and G. W. Watson, *The Journal of Physical Chemistry C*, 2008, 112, 9903-9911.
86. F. Murnaghan, *Proceedings of the national academy of sciences of the United States of America*, 1944, 30, 244.

Accepted Manuscript

87. H. J. Monkhorst and J. D. Pack, *Physical Review B*, 1976, 13, 5188.
88. V. Stevanovic, S. Lany, X. Zhang and A. Zunger, *Phys. Rev. B*, 2012, 85.
89. J. J. Carey and M. Nolan, *J. Mater. Chem. A*, 2017, DOI: 10.1039/C7TA00315C.

Accepted Manuscript